J. Fluid Mech. (2003), *vol.* 487, *pp.* 345–365.
DOI: 10.1017/S0022112003004750 Printed in the United Kingdom

Water wave attenuation due to opposing wind

By WILLIAM L. PEIRSON[1], ANDREW W. GARCIA[2] AND STEVEN E. PELLS[1]

[1]Water Research Laboratory, School of Civil and Environmental Engineering, The University of New South Wales, Sydney NSW 2052, Australia

[2]Coastal and Hydraulics Laboratory, United States Army Corps of Engineers, Vicksburg, Mississippi, USA

(Received 4 September 2002 and in revised form 4 November 2002)

A laboratory investigation of the attenuation of mechanically generated waves by an opposing wind has been completed. Wave attenuation was quantified by measurements of the decline in surface variance. These measurements show higher effective levels of monochromatic wave attenuation than predicted by air-side measurements: approximately an order of magnitude higher than measurements by Young & Sobey (1985) and, a factor of 3 higher than those of Donelan (1999) for waves in a JONSWAP spectrum. Furthermore, they show that theoretical estimates currently underestimate the attenuation rates by a factor of at least 3. This study has shown that the magnitude of wave attenuation rates due to opposing winds is approximately 2.5 times greater than the magnitude of wave growth rates for comparable wind forcing. At high wave steepnesses, detailed analysis suggests that air-side processes alone are not sufficient to induce the observed levels of attenuation. Rather, it appears that energy fluxes from the wave field due to the interaction between the wave-induced currents and other subsurface motions play a significant role once the mean wave steepness exceeds a critical value. A systematic relationship between the energy flux from the wave field and mean wave steepness was observed. The combination of opposing wind and wind-induced water-side motions is far more effective in attenuating waves than has previously been envisaged.

1. Introduction

Correct forecasting and hindcasting of waves generated by severe weather systems is of paramount importance to maritime interests and coastal residents because of the hazards to life and property. The most severe wave states are generated and modified by rapidly changing wind systems associated with the turning wind field and moving core of a tropical cyclone. Such wave systems are not modelled well by contemporary operational wave models (Hasselman *et al.* 1998). Moreover, the wave climate radiated by these systems is critically dependent on the region of most intense wave generation, which is close to the centre of the storm. Conditions in which the direction of the wind and waves do not coincide are a common feature of the open ocean. In coastal regions, offshore winds (opposing the incoming waves) can significantly alter the coastal wave regime. Offshore squall fronts also generate surface winds with rapidly changing direction, thereby modifying the local wind-wave generation regime.

Theoretical and laboratory studies of wind-wave generation have focused primarily on the growth phase, that is, with waves travelling in a direction predominantly aligned with the generating wind. Belcher & Hunt (1998) have reviewed airflow over waves and consequent wind-wave generation. They observed that theoretical and numerical predictions of growth rates are a factor of 2 to 3 smaller than measured growth rates.

Recent field measurements (Wright *et al.* 2001) have provided detailed depictions of wave spectra in a tropical cyclone and focused attention on the importance of wave response when the wave direction is not aligned with the wind. Nine spectra were acquired in the lower left quadrant (southwest quadrant) of the cyclone. Of the nine spectra, only one showed the direction of the peak wave energy to be within 90° of the dominant wind. The remaining eight showed the peak wave energy propagating from 90° to 180° to the wind direction. Surface wind speeds at the locations where these spectra were measured ranged from $9\,\mathrm{m\,s^{-1}}$ to $35\,\mathrm{m\,s^{-1}}$ and significant wave heights ranged from 4.4 m to 5.9 m. The greatest wind speed and significant wave height observed in this storm were $42\,\mathrm{m\,s^{-1}}$ and 10.9 m respectively, both in the upper right (northeast) quadrant. At some measurement locations, two, and sometimes three, distinct wave fields could be identified. The occurrence of distinct and separate wave fields was much more frequent in the lower (southern) half-sector of the storm. One interpretation of this observation is that the lower half-sector is a region where both wave generation and wave attenuation by wind occur and may be the area where mariners describe the seas as 'confused'.

An earlier investigation by Bowers, Morton & Mould (2000) of wind and wave directionality in North Sea storms suggests that for some types of floating platforms, maximum mooring forces do not occur when the wind and waves are aligned, but when the angle between wind and waves is in the range of 60°–90°. This condition tends to occur during the growth and attenuation phases of the storm when swell and locally generated sea are not directionally collinear with the wind. Observed angles between wind and swell direction during the growth phase was as much as 149°, and as much as 172° during the attenuation phase. Moreover, as with Wright *et al.* (2001), the wave spectra observed by Bowers *et al.* (2000) during the storm growth and attenuation phases were multi-peaked.

In comparison with the growth phase, there has been relatively little investigation of wind forcing from directions other than that aligned with the wave direction. The observations of Wright *et al.* (2001) have shown that such investigations would be appropriate, given the complexity of wind–wave interaction within intense low-pressure systems, which is usually the cause of the most hazardous sea states.

Prompted by these field observations of the complex and apparently closely coupled behaviour of wind and waves within intense storms and that relatively few laboratory studies have examined the effects of wind in directions other than aligned with that of the waves, we have undertaken a laboratory investigation of the mechanically generated wave response to an opposing wind. Wave attenuation has been quantified by measurements of surface variance – such a study has not previously been reported in the open literature.

2. Previous studies

Many field and laboratory measurements of wave growth and attenuation due to wind have been based on correlating pressures in the air immediately above the waves with their surface slope. There are at least two key assumptions in this

approach:

1. The primary process responsible for wave growth and attenuation is form drag induced by the wind.

2. Since surface pressures inducing energy fluxes cannot be measured directly, it is assumed that the surface pressure can be extrapolated from measured pressures some distance above the wave surface. This is in spite of flow visualization work of Kawai (1981) and Banner & Peirson (1998) who have shown that flow separation regions adjacent to the surface can be very compact. These regions may be difficult to penetrate even with surface-following probes.

Surface pressure–slope correlation measurements of wave growth and attenuation were initiated by Longuet-Higgins, Cartwright & Smith (1963) and have been followed by studies by Shemdin & Hsu (1967), Dobson (1971), Snyder *et al.* (1981), Young & Sobey (1985), Banner (1990), Hasselman & Bösenberg (1991), Mastenbroek *et al.* (1996) and Donelan (1999, hereafter referred to as D99), amongst others.

Using correlations of near-surface air pressures with surface slopes, Snyder *et al.* (1981) found that that open-ocean decay rates due to opposing winds were roughly an order of magnitude smaller than wind-generated wave growth rates. Hasselman & Bösenberg (1991) found that the attenuation rates due to opposing winds were too small to be measured. Laboratory measurements by Young & Sobey (1985) using similar techniques also found that attenuation rates are very small in comparison with growth rates.

In contrast, recent theoretical estimates (Harris, Fulton & Street 1995; Mastenbroek 1996; and Cohen 1997) using k–ε and second-order turbulence closure models predict that attenuation rates should be substantially higher than indicated by both the field and laboratory studies. The results of these theoretical studies give mutually consistent levels of attenuation (see figure 6).

D99 has reported wave growth and attenuation rates obtained using pressure measurements in the air using a surface-following probe moving vertically above groups of laboratory waves generated with a JONSWAP spectrum. This instrument was designed to allow a small pressure probe to track the motion of the surface, remaining a small (unspecified) distance above the water. Extrapolation of the measured pressures was still required to derive the actual surface pressures. D99 found that the estimated wave attenuation rates were approximately 40% of the growth rates.

Although relatively few studies of wave attenuation by opposing winds have been undertaken, a related investigation of wind drift in the presence of opposing swell has been undertaken by Cheng & Mitsuyasu (1992, hereafter referred to as CM92). They found that the wind-induced drift was higher when expressed as a proportion of the friction velocity in the air $u_*^a (= \sqrt{\tau/\rho_{air}}$, where τ is the total wind stress and ρ_{air} is the density of air) for the adverse wave case than for the case where the wind and waves are in the same direction. This was in spite of the Lagrangian drift associated with the mechanical waves being opposed to the wind-induced drift.

CM92 also measured wind drag coefficients and wave spectra. They found a weak dependence of the drag coefficient (and by implication the roughness length in the air) on the paddle wave steepness and direction of low-frequency wave propagation. The energy of small wind waves is substantially reduced in the presence of lower-frequency paddle waves travelling in the direction of the wind. In contrast, CM92 found that, in the presence of opposing swell, there is little or no attenuation of the wind waves and a substantial increase in wind-wave energy under light winds.

In our study, we measured the surface wave field to obtain estimates of wave attenuation due to an opposing wind. By measuring the change in wave energy along

a wind-wave tank, wave attenuation rates can be obtained directly. The aim was to provide results comparable to previous laboratory studies based on air pressure–surface slope correlations. Direct measurement of the wind-induced growth of low-frequency paddle waves has been accomplished successfully by Bole & Hsu (1967) and Mitsuyasu & Honda (1982, hereafter MH82).

3. Method

3.1. *Theory*

The diversity and duplication of notation within the air–sea interaction literature is a source of continuing confusion. In this paper, we follow the notation of Komen *et al.* (1994, especially Section I.2.5, p. 25*ff*).

The local total energy density of surface waves propagating past a point can be evaluated from

$$E = \rho_w g \langle \eta^2 \rangle = \rho_w g \int\int F(f,\theta)\,\mathrm{d}f\,\mathrm{d}\theta, \tag{1}$$

where E is the total local energy density, ρ_w is the density of water, g is gravitational acceleration, η is the instantaneous water surface elevation and the angle brackets indicate time-averaging and F is the spectral energy density as a function of wave direction θ and wave frequency f. In this investigation, we were concerned with the development of paddle wave energy along the axis of a laboratory tank. Directional components need not be considered.

The wave energy balance equation is (for example, Komen *et al.* 1994, pp. 33 and 47)

$$\frac{\mathrm{d}F(f,\theta)}{\mathrm{d}t} = S_{in}(f,\theta) + S_{nl}(f,\theta) + S_{diss}(f,\theta), \tag{2}$$

where S_{in} is the energy input from the wind, S_{nl} are nonlinear energy transfers due to wave–wave interactions and S_{diss} (a negative quantity) is the loss of energy from the wave field. Note that the above equation uses the total derivative and therefore considers changes moving with the group velocity of the waves.

When the wind is in the same direction and has a higher speed than the propagating waves, the ensuing drag on the waves will result in a positive energy flux to the wave field, S_{in}. In the case where the directions of the wind and the waves are opposed, the surface stress vector and the wave vector are opposite in sign and there cannot be an energy flux to the waves.

S_{nl} describes the transfers of energy among different wave frequencies within a wave spectrum. Interacting directional spectral components are essential for nonlinear transfers to occur. Here, we are considering the behaviour of monochromatic, monodirectional waves that have a relatively low frequency in comparison with any wind-generated waves. The effects of nonlinear interactions among the wind-generated microscale waves may be important but nonlinear interactions are negligible for wind-forced low-frequency monochromatic waves (Bliven, Huang & Long 1986). Consistent with the findings of Bliven *et al.* (1986), although the direction of the applied wind was opposite to that in our experiments, the spectra obtained during this investigation (for example, figure 2*a*) show no evidence of the development of Benjamin–Feir sidebands.

Changes in surface wave energy due to dissipative processes (S_{diss}) are generally attributed to wave breaking or interactions between the waves and fluid boundaries.

This investigation addresses the attenuation of deep-water waves due an opposing wind. For attenuation to occur, energy must be lost from the wave field to either the air above or the water column below. Breaking does not occur at the scale of the paddle-generated waves considered here. Theories for the loss of wave energy due to viscosity have been experimentally verified by the studies of MH82 and their results were used in this investigation. Wave attenuation rates due to viscous effects were deducted from the measured attenuation rates during this study so that the attenuation directly attributable to wind-induced effects can be obtained.

Donelan (1990) has observed that freely propagating waves can transfer energy to the air above to create wave-driven winds. However, in the presence of an opposing wind, the stress applied by the wind implies a downward energy flux and if there is to be any upward energy flux from attenuating waves, this energy can only be transferred to generate turbulence in the air immediately adjacent to the surface.

There appear to be two ways in which wave energy can be transformed into kinetic energy in the water column below. First, Longuet-Higgins (1969) showed that the interaction between local surface stresses and the surface orbital velocities of a larger-scale wave can contribute to or diminish wave energy. To our knowledge, there has been little direct measurement of this process and its potential contribution to the growth or attenuation of surface waves, except during the estimation of wave-coherent tangential stresses along the surfaces of microscale-breaking wind waves by Banner & Peirson (1998). Numerical estimates by Mastenbroek (1996) indicate that tangential stress could contribute approximately 30% of the total attenuation of waves due to an opposing wind.

Secondly, energy fluxes from the wave field can occur due to wave–current and wave–turbulence interactions. Belcher, Harris & Street (1994) reported that their analytical model showed that wave growth rates were reduced by a factor of 2 when turbulence in the water was included. Teixeira & Belcher (2002) developed a rapid-distortion model of wave–turbulence interactions and concluded that the presence of turbulence not immediately in the vicinity of the interface could also make a non-negligible contribution to wave attenuation.

Laboratory studies of wave–turbulence interactions have been undertaken by a number of investigators, including Cheung & Street (1988), Jiang, Street & Klotz (1990) and Thais & Magnaudet (1996). Studies of this type require sophisticated techniques to distinguish between mean, orbital and turbulent motions beneath the waves. To date, such studies have been restricted to the investigation of velocity structure below the level of the wave troughs. The work by Thais & Magnaudet (1996) is the most comprehensive to date and they investigated wind-ruffled paddle waves with a steepness of approximately 0.1 with the wind direction aligned with the wave direction. They found turbulence levels up to an order of magnitude higher than levels adjacent to solid walls. Their results suggested that the turbulence is directly forced by the wave-induced motion. They concluded that critical turbulence production was occurring within or at the surface of the wave crests. Unfortunately, they were not able to quantify the total energy flux from the wave field to the mean or turbulent velocity fields.

For our experiments, in which low-frequency, monochromatic, monodirectional waves of frequency f_p were investigated in the absence of wind energy input and nonlinear interactions, equation (2) reduces to

$$\frac{\mathrm{d}F}{\mathrm{d}t} = S_{diss}, \tag{3}$$

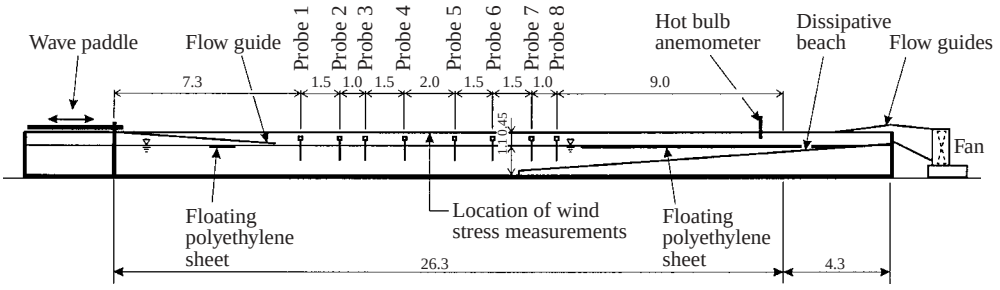

FIGURE 1. Layout of the test facility: approximate scaling 1 : 300; dimensions in metres.

and this equation is only applied to waves of frequency f_p travelling in an upwind direction. S_{diss} is composed of two components:

$$S_{diss} = S_{attn} + S_{visc}, \tag{4}$$

where S_{visc} is the viscous attenuation rate of the waves due to interaction between waves and the surface and the sidewalls; and S_{attn} is the attenuation rate of the waves due to the wind and is composed of potential contributions of wave energy flux to air- and water-side motions.

3.2. *Measurement techniques*

Bole & Hsu (1969) and MH82 used ensemble measurements of the increase in surface mean-square deviation (equation (1)) in the wind direction at a sequence of points along a wave tank to quantify the development of wave energy due to wind action. These measurements showed an increase of wave energy with distance.

If a wave packet exposed to a steady wind does not change its group speed rapidly with time, we can evaluate the local time-dependent wave growth rate as

$$\frac{\mathrm{d}F}{\mathrm{d}t} = \frac{\partial F}{\partial t} + c_g \frac{\partial F}{\partial x} = c_g \frac{\partial F}{\partial x}, \tag{5}$$

where c_g is the group wave speed (the speed at which wave energy propagates) and x is distance in the direction of the low-frequency wave propagation. For deep-water waves, $c_g = c/2$, where c is the wave phase speed. In these experiments, we have used a steady wind and $\partial F/\partial t = 0$. Wave growth rates are usually expressed in a time-based dimensional form as $\gamma = (1/F)(\mathrm{d}F/\mathrm{d}t)$ or as the non-dimensional quantity γ/f. A difficulty with this technique is that as well as developing low-frequency waves, the wind also generates a spectrum of high-frequency microscale waves ($0.05\,\mathrm{m} < \lambda < 0.4\,\mathrm{m}$). MH82 extracted the growth rate of the low-frequency waves ($f_p < 1.3\,\mathrm{Hz}$, $\lambda > 0.8\,\mathrm{m}$) using spectral filtering techniques. In this investigation, we have applied the techniques of MH82 to the case where the wind is in opposition to the propagating low-frequency waves. Here, a wind-related wave attenuation rate is to be determined which is denoted by γ_a, where $\gamma_a = -\gamma$.

3.3. *Wind-wave facility*

The experiments were undertaken in a wind-wave tank at the Water Research Laboratory. Overall tank dimensions are length 30 m, width 0.9 m and height 1.55 m. The layout of this facility is shown in figure 1. Waves are generated by a controlled random generator at one end of the tank. During these investigations, only mono-chromatic waves were investigated. At the far end, a dissipating beach was installed. The tank is roofed and flow in the air cavity is generated by a large fan fitted at the

opposite end to the wave generator. For these investigations, water depth in the tank was 1.10 m, giving an air cavity depth of 0.45 m (identical to MH82 and CM92). Wind speeds in the air cavity were monitored using a hot bulb anemometer supported by the roof at mid-height within the air cavity.

We encountered some particular experimental difficulties which do not appear to have been discussed by other researchers. For both wave growth and attenuation measurements, reflected waves can contaminate the measurements. In the case of wave growth measurements, reflected waves will be exposed to an opposing wind which will attenuate them as they progress down the tank towards the paddle. The attenuation of the reflected waves will contribute to the total local wave energy, thereby creating apparent additional growth. The waves incident on the dissipating beach will be the largest (and therefore, steepest) waves in the tank, which is the preferred condition for maximum wave dissipation (CERC 1984, pp. 2–118). Provided that the reflected waves contain less than a few percent of the incident wave energy and the attenuation rate is at least comparable with the growth rate, this will not induce significant error.

For wave attenuation measurements, the problem is more significant. The incident waves at the beach are relatively small compared to those generated at the paddle and the dissipation of smaller waves at beaches is a less efficient process (CERC 1984, pp. 2–118). Reflected waves from the beach will grow under the action of the wind, inducing an apparent higher attenuation rate. Such a problem will be exacerbated if there is a substantial length of tank between the point of the final measurement and the point of first contact between wind and water. If the attenuation rate is small in comparison with the growth rate, it may not be possible to measure the attenuation rate.

For our experiments, we addressed this problem as follows. A thin polyethylene sheet was floated on the surface of the water from approximately 1 m upwind of the wave probe nearest the fan. This had two effects: waves propagating towards the beach were subject to surface dissipation from the point of entry beneath the sheet, thereby enhancing the dissipative effect of the beach and preventing reflected waves from growing whilst propagating from the beach to the point of measurement. This technique also provided a long development length for the air flow in the upper cavity. By pulsing the wave generator, we showed that the reflected waves generated by the incidence of small paddle waves were reduced to less than 2% of the incident wave amplitude. Reflected waves were indistinguishable amongst the (small, $<2\%$) cross-tank oscillations that were also generated. Given the large dissipation rates that were measured, this effect was not significant.

Another problem occurs at the other end of the tank. Small wind waves generated in the opposite direction develop to higher amplitudes and lower frequencies as they propagate away from the fan. These will reflect from any surface-piercing paddle with approximately 100% reflection and potentially contaminate the attenuation measurement. If the paddle waves are of relatively high frequency and the tank is long, the wind waves can develop a frequency comparable with the paddle waves. D99 addressed this problem by using a submerged wave generator and installing a dissipative beach behind the wave generator. This approach has its difficulties: waves propagate in both directions away from wave generators and unwanted out-of-phase wave components may be generated by reflections from the beach behind the generator, particularly if the paddle waves are of low frequency. We developed an alternative method which proved effective in alleviating this problem. In addition to the polyethylene sheet installed at the upwind end of the tank described previously, we floated a short (1 m) sheet of polyethylene approximately 3 m from the paddle.

	This study: wind and paddle waves ($ak_0 = 0.125$, $f_p = 1.0$ Hz)		This study: wind waves only		CM92: wind and paddle waves ($ak_0 = 0.125$, $f_p = 1.02$ Hz)		CM92: wind waves only	
U_{cl} (m s^{-1})	u_*^a (m s^{-1})	z_0 (mm)	u_*^a (m s^{-1})	z_0 (mm)	u_*^a (m s^{-1})	z_0 (mm)	u_*^a (m s^{-1})	z_0 (mm)
5	0.237	0.036	0.192	0.0068	0.25	0.084	0.25	0.084
7	0.324	0.035	0.315	0.034	0.33	0.069	0.38	0.18
9	0.478	0.129	0.422	0.049				
11	0.625	0.221	0.579	0.147				
15	1.103	1.083	1.050	0.846				

TABLE 1. Summary of air flow measurements from this study and CM92. U_{cl} is wind speed, u_*^a air friction velocity, and z_0 roughness length in the air.

This proved effective in entirely dissipating the short wind waves whilst its effect in attenuating the paddle-generated waves or disturbing their form was very small.

Local measurements of the wind stress were obtained by measuring the near-surface logarithmic boundary layer profiles in the air for each wind speed condition, U_{cl}. These were taken at the mid-point of the wave measurement section in the presence and absence of paddle waves with frequency 1.0 Hz and non-dimensional wave steepness at the paddle of $ak_0 = 0.125$. The results of the wind stress measurements are shown in table 1 with corresponding values derived from the logarithmic wind profiles in CM92. Our measurements indicate friction velocity measurements u_*^a consistent with CM92 although our measured z_0 values are somewhat lower. The z_0 values are not critical to this study and will not be discussed further. Our measurements also indicate a slight and systematic increase in u_*^a in the presence of paddle waves although we estimate the measurement error in u_*^a to be 10%. For all normalizations of our data involving u_*^a, we have taken u_*^a values from the leftmost column in table 1 at the corresponding wind speed.

During this investigation, water surface elevations were monitored using capacitance wave gauges fitted with fine ($\sim$200 μm diameter) wire filaments. Each gauge had a range of approximately 200 mm. These were carefully and regularly calibrated and over the period of testing showed a gain repeatability better than 2%. Eight probes were used, located at distances of 1.5, 2.5, 4.0, 6.0, 7.5, 9.0 and 10.0 m from the first probe within the roofed section (see figure 1). The water surface elevation measurements of the wave probes were recorded at a frequency of 40 Hz per channel by a computer with an analogue-to-digital converter. These data were stored for subsequent processing.

3.4. *Data processing*

Fast Fourier transforms (FFTs) were used to process 2048 data points from each record (approximately 50 s) to determine the local wave energy. Representative wave probe array spectra containing relatively steep waves are shown in figure 2. This was obtained for conditions of $f_p = 0.91$ Hz at $U_{cl} = 7$ m s^{-1}, $ak_0 = 0.19$ (panel *a*) and $U_{cl} = 15$ m s^{-1}, $ak_0 = 0.12$ (panel *b*).

As noted earlier, wind waves are not attenuated by opposing swell. Consequently, the surfaces of the low-frequency paddle waves are covered by microscale waves. Figure 3 is a photograph of a representative condition ($U_{cl} = 7$ m s^{-1}, $ak_0 = 0.19$, $f_p = 1.1$) taken between probe positions 6 and 7. In all of our experiment conditions,

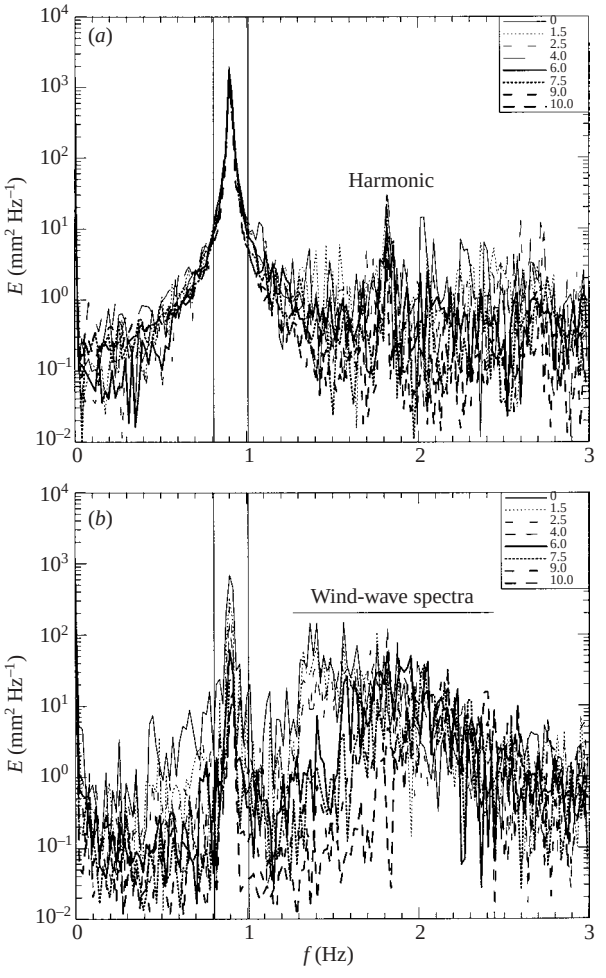

FIGURE 2. Representative wave spectra. Individual wave spectra are indicated by different line styles indicated by the legend at top right with the value indicating the probe position. The frequency bands used to extract paddle wave energy are indicated by the vertical lines. (*a*) $f_p = 0.91$ Hz, $U_{cl} = 7\,\mathrm{m\,s^{-1}}$, $ak_0 = 0.19$; (*b*) $f_p = 0.91$ Hz, $U_{cl} = 15\,\mathrm{m\,s^{-1}}$, $ak_0 = 0.13$.

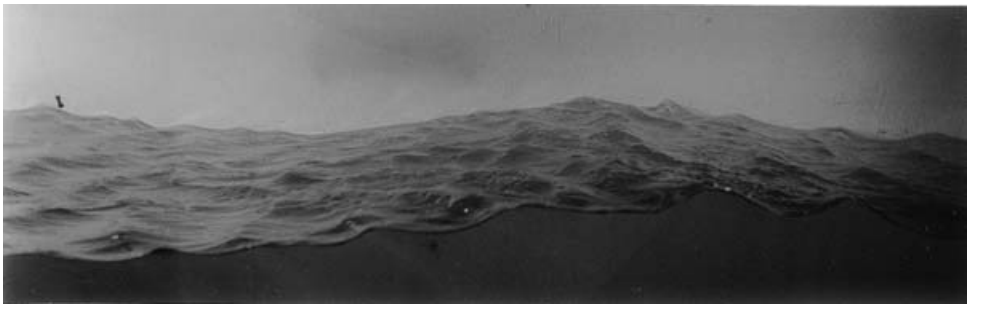

FIGURE 3. Photograph of the tank surface at a location between probes 6 and 7 for paddle waves of $f_p = 1.11$ Hz, $ak_0 = 0.19$ exposed to a wind in the upper cavity of $U_{cl} = 7\,\mathrm{m\,s^{-1}}$. Note the presence of microscale waves over the entire wave surface with steeper waves on the crest of the lower-frequency paddle wave. The low-frequency paddle wave is travelling from left to right and the wind is from right to left.

microscale breaking waves were present along the surfaces of the underlying low-frequency paddle waves. Figure 3 shows the entire surface to be populated with microscale waves, with steeper waves on the crest of the low-frequency paddle wave.

Energy was extracted from the low-frequency waves by integrating the energy within a frequency band between $(1 \pm 0.1) f_p$. The frequency band was selected to be as narrow possible to ensure that energy associated with the high-frequency wind waves was not included. Figure 2 illustrates the effectiveness of this approach in retaining critical energy components whilst removing the wind-wave energy. In both cases, the energy associated with the fundamental frequency is captured, with energy levels falling to approximately 1% of the peak value at the frequency band limits. In figure 2(a), there is no clear wind-wave spectrum, due to the relatively light wind, but the harmonic of the low-frequency waves is clearly apparent. Nonetheless the peak energy associated with the harmonic that is eliminated by the filtering process used in the attenuation measurements is only approximately 1% at the fundamental frequency. In figure 2(b), the wind-wave spectra are clearly apparent and excluded by the imposed frequency band limits.

To quantify γ_a from point measurements of wave energy along the tank, a model of wave attenuation must be fitted to the data. Consistent with previous investigators, we assume exponential attenuation:

$$E = E_0 \mathrm{e}^{-\Delta x}. \tag{6}$$

In each case, Δ was determined from the measured data by a least-squares fit of this equation to the measured energy as a function of fetch. Non-dimensional attenuation rates were determined from

$$\frac{\gamma_a}{f} = -\frac{\dot{E}}{fE} = -\frac{c_g}{fE}\frac{\partial E}{\partial x} = \frac{(\Delta - \Delta_{visc})c}{2f}, \tag{7}$$

where Δ_{visc} is the estimated attenuation rate due to viscosity at the surface and the walls of the tank based on the work of Van Dorn (1966). The tank used in the experiments is substantially wider than that used by MH82 and dissipation rates in the absence of wind were so low that it was impossible to measure these with confidence. The process of least-squares fitting yields a correlation coefficient r which can be related to a confidence interval for Δ of

$$\pm \frac{t^p \sqrt{1 - r^2}}{\sqrt{n - 2}} \frac{\sigma(\ln(E/E_0))}{\sigma(x)},$$

where t^p is the value from the *Student's t distribution* for confidence limits of p%, σ signifies the standard deviation and x the positions of n wave probes (see Acton 1959, p. 24). For this investigation we selected $p = 90\%$.

4. Results

Measurements were completed for five wave paddle frequencies (0.77, 0.87, 0.91, 1.11 and 1.43 Hz), three nominal wave steepnesses ak_0 (0.06, 0.13 and 0.19) and four wind speeds ($U_{cl} = 5, 7, 9, 11\,\mathrm{m\,s^{-1}}$ with a single data point at $U_{cl} = 15\,\mathrm{m\,s^{-1}}$). However, not all combinations of conditions could be tested. For lighter winds and lower paddle frequencies, the attenuation rate was small compared to its confidence limits and the result was inconclusive. For stronger winds and higher paddle frequencies, the attenuation rate was so great that the paddle wave energy could not be distinguished from amongst the wind-wave energies at those probes furthest from the paddle

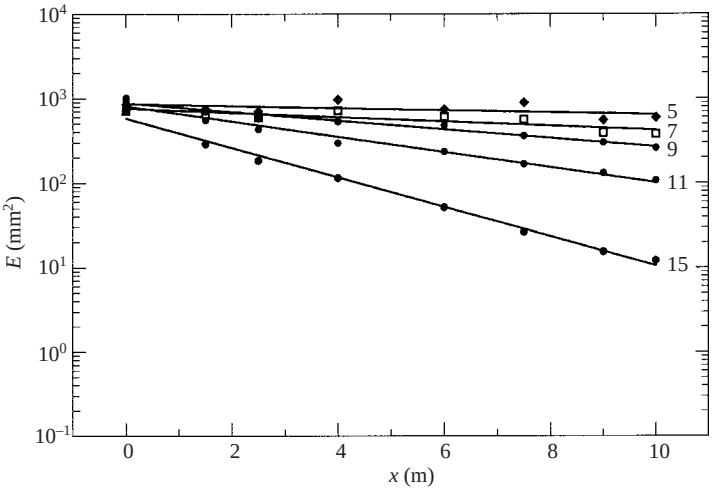

FIGURE 4. Paddle wave energy as a function of distance along the tank at a single paddle setting with $f_p = 0.91$ Hz and $ak_0 = 0.13$. Solid lines indicate best-fit lines to the data. Wind speeds are indicated by the numbers to the right of each data set.

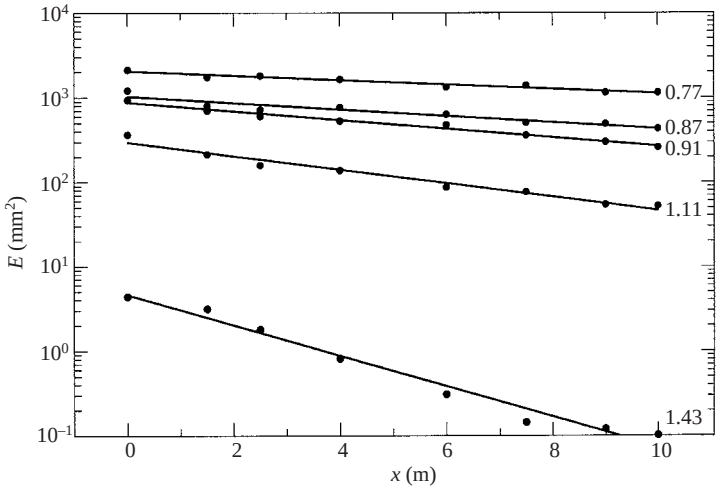

FIGURE 5. Paddle wave energy as a function of distance along the tank with a nominal steepness at the paddle of $ak_0 = 0.13$ and $U_{cl} = 9\,\mathrm{m\,s^{-1}}$. Solid lines indicate best fit lines to the data. Values of f_p are indicated by the numbers to the right of each data set.

yielding large confidence limits for the determined attenuation rates. Figures 4 and 5 illustrate representative results of the decline in paddle wave energy with distance due to the opposing wind. Figure 4 shows the change in attenuation rate in response to increasing wind forcing whilst the increasing attenuation rate with increasing paddle wave frequency at a single wind speed is illustrated in figure 5.

As shown in figures 6 and 7, significantly higher attenuation rates have been measured during this investigation than are predicted on the basis of laboratory measurements of wave-induced pressures in the air or by theoretical studies. Figure 6 shows non-dimensional attenuation rates (γ_a/f) as a function of the ratio of the friction velocity in the air and the wave speed u_*^a/c (similar to the approach to growth

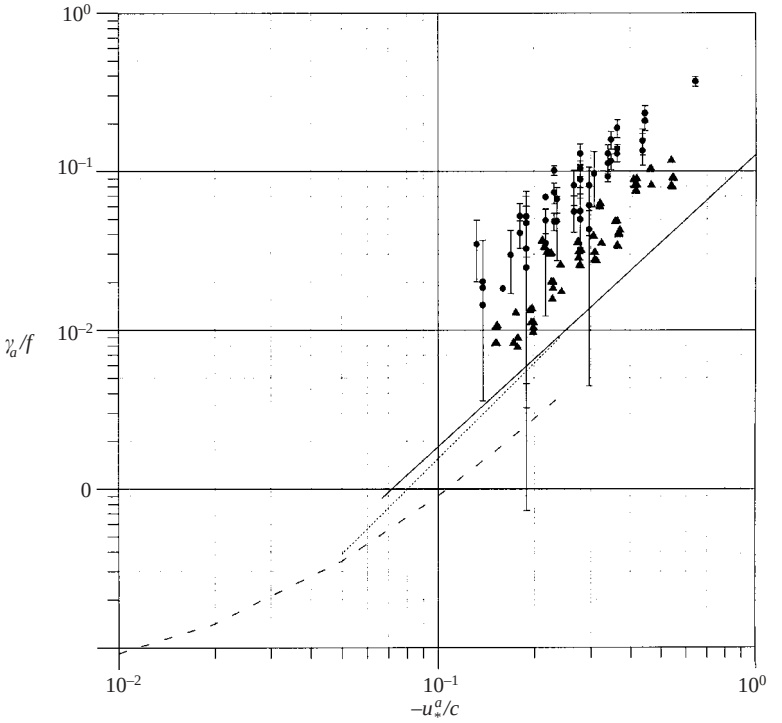

FIGURE 6. Non-dimensional attenuation rates as a function of the ratio of air friction velocity to wave speed. The results of this investigation are indicated by the solid circles with 90% confidence intervals as shown. The dashed line is the result from Young & Sobey (1985) for $ak = 0.1$. The dotted line and solid lines show the results of Harris *et al.* (1995) and Cohen (1997) respectively. For comparison with wind-wave growth rates, the results of MH85 are shown as solid triangles with γ/f as a function of u_*^a/c imposed on the same axes.

rate data by Plant 1982). The data are presented in figure 6 with other relevant wave attenuation studies.

Based on the Young & Sobey (1985) measured relationship of $U_\infty \approx 30u_*^a$ (derived from data presented in their paper), their equation (31) has been replotted over the range indicated in their figure 10 and is also shown in figure 6. This curve was calculated for a representative value of $ak = 0.1$. As shown, the curve estimated from the Young & Sobey (1985) measurements is up to a factor of 2 lower than comparable theoretical studies and approximately one order of magnitude smaller than the results of this investigation.

Harris *et al.* (1995) completed numerical simulations of airflow over a wave travelling in the opposite direction to the wind using a k–ε turbulence model. They simulated the experiment conditions of Young & Sobey and found higher phase shifts in the surface pressure distribution than had been measured. Their results are also shown in figure 6 and wave attenuation rates up to a factor of 2 higher than Young & Sobey (1985) are predicted. Their attenuation estimates are between 5 and 10 times smaller than the results measured in this study.

Cohen (1997) has undertaken simulations with a simplified second-order turbulence closure model of wave attenuation due to an opposing wind. This model reproduced the limited wave attenuation results of the more sophisticated model of Mastenbroek (1996). Cohen concluded that attenuation rates should be much higher than suggested

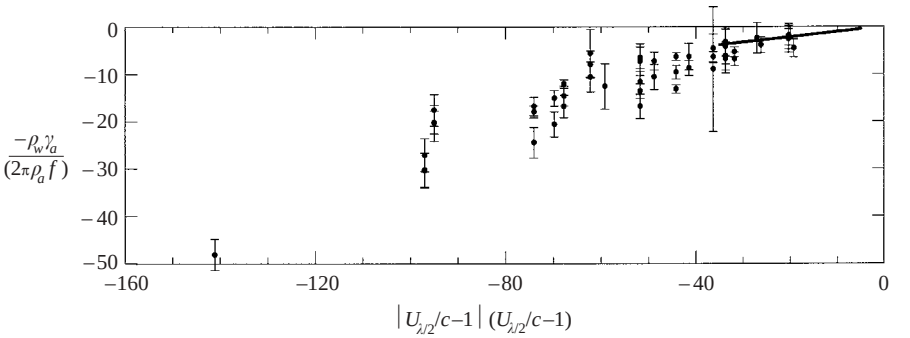

FIGURE 7. Comparison of measured attenuation rates with the best fit presented in D99 to attenuation rates derived from pressure measurements in the air. Solid circles are the values measured during this investigation with the 90% confidence intervals for each point shown.

by Young & Sobey. As shown in figure 6, there are only minor differences between Cohen's results and those of Harris *et al.* (1995).

The data from the present investigation have been summarized and presented in an identical form to those above and are also shown in figure 6. Possible error is indicated by bars showing the 90% confidence interval of these measurements. The range of scatter in this normalization is over a range of a factor of approximately 3. However, the confidence limits indicate that this scatter is unlikely to be entirely due to measurement uncertainty. The measured attenuation rates are far higher than has been suggested by previous studies. The closest estimates are those of Cohen (1997) but the measured values are still a factor of 4 to 10 higher. As noted in the introduction, measured values of wave growth are approximately a factor of 2 to 3 higher than theoretical and numerical estimates of wind-induced wave growth (Belcher & Hunt 1998).

MH82 measured the wind-induced growth rates of waves of the same scale exposed to wind forcing using the same techniques. In figure 6, these measured wind-induced growth rates are superimposed as solid triangles with the non-dimensional growth rate γ/f presented as a function of u_*^a/c at the same scale. In this form, it can be observed that the wind-induced attenuation rates are approximately 2.5 times higher than the growth rates of waves of comparable scale.

Unfortunately, there is insufficient supporting data in D99 for that data set to be compared directly with those shown in figure 6. However, using the format of D99, the data of the present study can be compared with these pressure-based measurements above groups of waves with JONSWAP spectra (figure 7). The attenuation rates measured during this investigation appear to be higher by a factor of 1.5 than D99 over the relatively small range of $U_{\lambda/2}/c - 1$ used by D99. D99 suggested a quadratic relationship between the non-dimensional energy flux and $U_{\lambda/2}/c - 1$, whereas the wider measurement space of our data set indicates that the behaviour is approximately cubic. Consequently, extrapolation of the results of D99 to values of $U_{\lambda/2}/c - 1$ with higher magnitude can increase the apparent disparity up to a factor of approximately 3 over the range of values considered in this study.

Within our data set, a systematic increase in attenuation rate as a function of wave amplitude was observed. Such behaviour for $U_{cl} = 9\,\mathrm{m\,s^{-1}}$ and $f_p = 0.91\,\mathrm{Hz}$ are shown in figure 8. Young & Sobey (1985) suggest that the non-dimensional attenuation rate (γ_a/f) increases quadratically with ak. In D99, a constant sheltering coefficient is

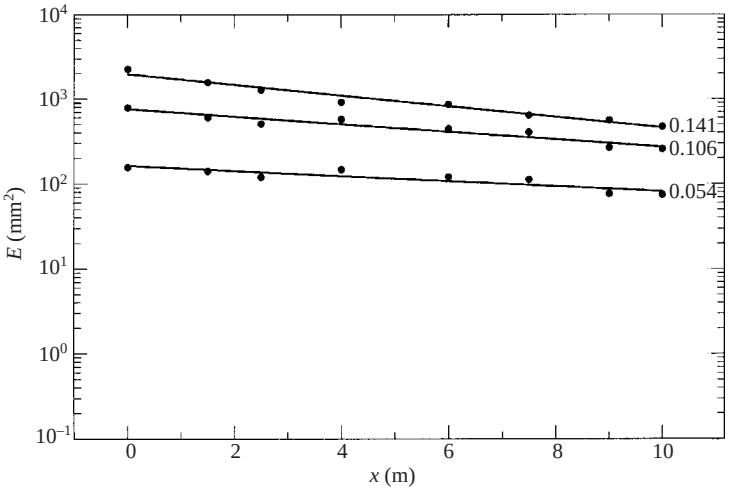

FIGURE 8. Paddle wave energy as a function of distance along the tank at various paddle settings and $U_{cl} = 9\,\mathrm{m\,s^{-1}}$, with $f_p = 0.91\,\mathrm{Hz}$. Values of ak at $x = 5\,\mathrm{m}$ are indicated by the values to the right of each data set. Solid lines indicate best-fit lines to the data.

suggested with no specific dependence on ak although it is noted that the likelihood of separation over a single sinusoid increases approximately as $ak(1 - c/U)^2$.

Theoretical studies usually express growth rates in the form of either:

$$\frac{\gamma}{f} = A(ak)^B \left(\frac{u_*^a}{c}\right)^c \tag{8}$$

or

$$\frac{\gamma}{f} = A(ak)^B \left(\frac{U}{c} - 1\right)^c \tag{9}$$

For example, Plant (1982) uses the form of equation (8) and determines

$$\frac{\gamma}{f} = (0.25 \pm 0.13) \left(\frac{u_*^a}{c}\right)^2; \tag{10}$$

no dependence of growth rate on wave steepness was determined.

In their wave growth measurements, MH82 endeavoured to determine a dependence of wave growth rate on wave steepness but no systematic relationship could be established. In calculating these normalizations, we have used the wave steepness at the mid-point of the measurement section ak rather than the nominal steepness at the wave paddle ak_0. This differs from the approach used by MH82 and use of ak_0 in their calculations may have masked a systematic relationship within measurements of rapidly growing waves.

Using similar forms for wave attenuation, we have been able to determine best-fit relationships for our data set. Relationships of the form of both (8) and (9) above were developed. Their performance is illustrated in figure 9 with the resulting forms being

$$\frac{\gamma_a}{f} = 2.275(ak)^{0.238} \left|\frac{u_*^a}{c}\right|^{2.112}, \tag{11}$$

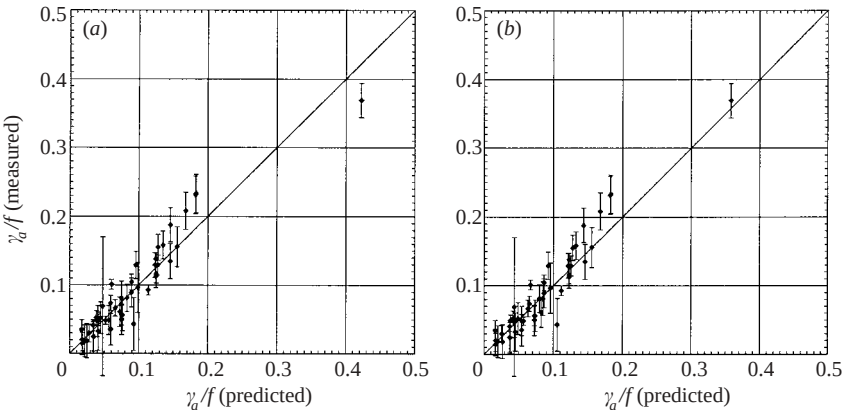

FIGURE 9. Comparison of measured attenuation rates with the values predicted by the fitted equations (11) and (12), (*a*) and (*b*) respectively. The 90% confidence intervals for each data point are shown.

$$\frac{\gamma_a}{f} = 0.000236(ak)^{0.240}\left|\frac{U_{\lambda/2}}{c} - 1\right|^{3.265}. \tag{12}$$

The root-mean-square residual obtained for equation (11) was 5% smaller than that for equation (12). However, as shown in figure 9, equation (12) seems to provide a slightly better visual fit to the data. It can also be observed that, except for a single data point, maximum differences between predicted and observed values are less than 20% beyond the 90% confidence interval.

Relationships were also determined using a wave Reynolds number (aU_{cl}/ν_{air}, not shown) rather than wave steepness in equations of the form of (11) and (12). The root-mean-square residuals were approximately 3% higher in both cases.

5. Discussion

There is a fundamental difference between the approach of this investigation and comparable numerical or air pressure measurement studies of wave attenuation by wind. Previous studies have been focused on the interaction between the air flow and the waves and have used these to deduce the wave attenuation response. In this study, the effect of wind and wave steepness on the attenuation rate of the waves has been measured directly. Substantially higher attenuation rates have been measured than have been predicted by corresponding numerical and laboratory studies. Also, this study has shown that attenuation rates of waves due to opposing winds are approximately 2.5 times greater than wave growth rates for comparable wind forcing. Effective attenuation rates of this magnitude have not previously been envisaged.

In deep water, wave breaking is currently deemed the primary contributor to the dissipation of wave energy. However, when opposing winds prevail within weather systems with rapid shifts in wind direction, they can continuously attenuate the exposed wave field.

5.1. *Potential tangential stress contributions*

As discussed in § 2, the laboratory studies using air pressure measurements invoke implicitly the assumption that form drag is the primary contributor to wave attenuation. Is it possible that the neglect of wave-coherent tangential stresses is

responsible for the disparity between our study and those employing air pressure–slope measurements to deduce wave attenuation rates? The numerical studies do not suggest that this is the case (for example, Mastenbroek 1996) and the relatively small values of ak that can be achieved by water waves do not permit the tangential stresses to contribute significantly to wave growth or attenuation.

Energy losses from the wave field arising from form drag are given by

$$\frac{\partial E}{\partial t} = -\tau_{form} c; \tag{13}$$

those arising from wave-coherent tangential stress are first order and of the form (see Longuet-Higgins 1969, p. 384):

$$\frac{\partial E}{\partial t} = -\tau_{tang} u_{orbital} \sim -\tau_{tang} akc. \tag{14}$$

Wave-coherent tangential stress can arise from local action of the skin friction on the surface (Banner & Peirson 1998) or from local stress concentrations generated by small-scale breaking along the surface of longer waves (Longuet-Higgins 1969). Note that the small microscale waves are breaking during these experiments and presumably attract significant form drag from the wind due to air-flow separation (Banner 1990 and Banner & Peirson 1998). More detailed studies of the air flow will be required to resolve the nature of the flow separation over these combined microscale and paddle-generated wave fields.

Generally, values of ak only rise above approximately 0.1 due to intense wind forcing or local convergence of wave energy density. This limit on the ak term severely restricts the ability of the wave-coherent tangential stress to contribute significantly to the wave attenuation process. (In our experiments, monochromatic waves were investigated thereby prescribing a level of low-frequency energy density and a mean wave steepness.)

It does not seem likely that neglect of the wave-coherent tangential stress can be responsible for the disparity between the observations of this study and complementary laboratory air-side measurements.

5.2. *Energy fluxes from the wave field to the air*

The wind direction and stress vector are both in the same direction so the energy flux from the wind is strictly downward. If the wave energy is transferred to the air by form drag or wave-coherent tangential stress, there must be enhanced turbulent dissipation in the air layers immediately above the surface to accommodate the combined input energy flux from the wind and the waves. However, the wind stresses and roughness lengths measured by MH82 (excepting those measurements where a surfactant was used) are very similar at the same wind speed to those measured by CM92 and during this study. This provides circumstantial evidence that there are no substantial changes to the turbulent structure in the air flow above the wave crests in comparison with the case where the wind and wave directions are aligned.

In addition, we have quantitatively examined the potential for form drag to be responsible for the observed attenuation. This has been accomplished by estimating the form drag implied by equation (13), assuming the observed attenuation rates are solely due to form drag. Using (13), we can determine that

$$\frac{\tau_{form}}{\tau_{tot}} = -\frac{1}{c\rho_{air} u_*^{a^2}} \frac{\partial E}{\partial t}. \tag{15}$$

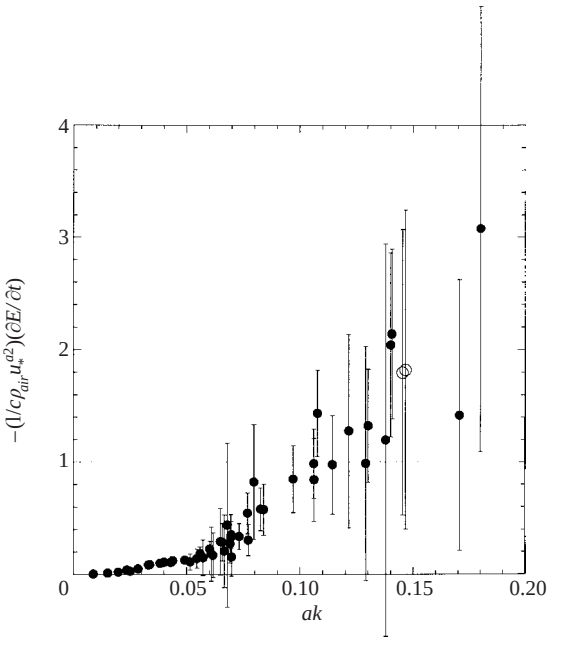

FIGURE 10. Rate of loss of wave energy as a proportion of the total wind stress presented as a function of wave steepness at the midpoint of the test section. Note that a value of 1 on the ordinate axis is the ceiling rate corresponding to the maximum wave attenuation achievable if the entire wind stress was mediated by form drag attenuating the paddle waves. Solid circles and open circles indicate measurements taken with air cavity depths of 450 mm and 790 mm respectively. Note that the measurements with the air cavity depth of 790 mm sit naturally amongst the other data and indicate that the results have not been influenced significantly by air cavity depth.

If the quantity on the right-hand side of (15) is plotted as a function of ak, as shown in figure 10, the data collapse and systematic behaviour can be observed. It appears that above a threshold of $ak = 0.06$, there is a more rapid rise in this non-dimensional attenuation rate. The best power-law curve fit to the data in figure 10 is given by

$$\frac{\partial E}{\partial t} = -115c\rho_{air}u_*^{a^2}\, ak^{2.2}. \tag{16}$$

Significantly, once $ak > 0.12$, the estimated values of τ_{form}/τ_{tot} using equations (15) and (16) become greater than unity. This implies that for $ak > 0.12$ the observed attenuation rate is greater than that that can be provided by form drag in the air. This finding was unexpected and prompted us to very carefully examine potential contributions from our selected experiment conditions.

We had selected our air cavity depth to correspond exactly to that used in the studies by MH82 and CH92. However, it appeared possible that the air cavity depth would create the opportunity for unwanted interactions between wave-induced pressure fields and the roof of the air cavity. We checked the possibility of interactions with the roof as follows. We increased the air cavity depth as much as possible without interfering with other aspects of the experiment. The water level was lowered by 340 mm thereby increasing the air cavity depth to 790 mm. Repeat measurements were taken at a wave steepness where the previous results had shown a greater wave attenuation rate than could potentially be supplied by form drag in the air. These were taken at a wind

speed of $7\,\mathrm{m\,s^{-1}}$, a wave frequency of 0.91 Hz and steepness of $ak = 0.145$. It was confirmed that the surface wind stress had not changed with the change in air cavity size by checking that the mean wind velocity remained unchanged from the previous experiments at a single point within the logarithmic layer above the surface.

The results with the significantly deeper air cavity have been superimposed on figure 10 where they sit naturally amongst the other data. Therefore, the limited air cavity depth required by the experiments has not had a significant effect on the measured results. In addition, these repeat measurements confirm wave attenuation rates greater than that achieved if the total wind stress was mediated entirely by form drag.

It therefore seems unlikely that the observed wave attenuation is due solely to the direct effects of wind-induced stresses along the paddle-generated wave surfaces.

5.3. *Energy fluxes from the wave field to subsurface currents and turbulence*

Energy fluxes from waves to the water are usually identified with wave breaking but for wave attenuation there is no breaking of the paddle-generated waves (figure 3). Energy fluxes from the waves to the subsurface currents and turbulence are possible due to interactions between waves and the wind-induced currents or between the waves and near-surface turbulence and discussed in § 3.1. The findings of CM92 show that the surface wind drift is significantly enhanced by the presence of low-frequency paddle waves travelling in an opposing direction to the wind. This result suggests a strong interaction between waves and subsurface current fields.

The strong wave attenuation rates observed in this study lend support to the suggestions of Belcher *et al.* (1994) and Thais & Magnaudet (1998) that significant energy fluxes from the wave field may occur due to wave interactions between the wave-induced velocities and the subsurface mean current and turbulent flow fields. However, the estimates of Belcher *et al.* (1994) and Teixeira & Belcher (2002) are at least a factor of 3 smaller than the values obtained during this study. The results of this investigation also suggest that above a threshold of wave steepness ($ak > 0.06$), these subsurface energy fluxes begin to dominate the attenuation of the waves. Below this threshold, wind-induced form drag could remain the primary contributor to the attenuation rate.

There can be significant differences between wind forcing for field and laboratory conditions. For example, under laboratory conditions typically $c/u_*^a \ll 10$ whilst for waves in the open ocean at the spectral peak values of $c/u_*^a > 10$ would be anticipated.

Whilst the normalizations of the data shown in figures 9 and 10 are consistent for the study data set, the implied attenuations of ocean swell by opposing winds are significantly different. For example, for swell with a peak spectra period of 10 s and an amplitude of 1 m when opposed by a wind of approximately $6\,\mathrm{m\,s^{-1}}$, the non-dimensional decay rate derived from equation (16) is approximately an order of magnitude smaller than that obtained from equation (11). Note that the normalization of conventional form (equation (11) and figure 9) suggests a very weak dependence on wave steepness (exponent ≈ 0.24) whilst figure 10 exhibits a strong dependence on wave steepness (exponent ≈ 2.2). Determination of appropriate forms for field conditions must await suitable studies utilizing field data sets.

6. Conclusions and recommendations

Measurements of the attenuation of wave energy due to an opposing wind obtained from direct measurement of the surface elevation have been obtained in this study. These show effective levels of wave attenuation that are approximately an order

of magnitude higher than predicted by the air-side measurements of Young & Sobey (1985) and a factor of 3 higher than those of D99 who used wave fields with a JONSWAP spectrum. Furthermore, they show that theoretical estimates also underestimate the attenuation rates by a factor of at least 3. Also, this study has shown that magnitude of wave attenuation rates due to opposing winds is approximately 2.5 times greater than the magnitude of wave growth rates at comparable wind forcing.

Systematic increases in wave attenuation rates with increasing wave steepness have been observed. Normalizations of the data based on wind forcing and wave steepness have been developed. This is in contrast with the observation that growth rate dependence on wave steepness could not be observed for waves travelling in the same direction as the wind (MH82). At high wave steepnesses, detailed analysis shows that it does not appear possible that the degree of attenuation observed can be due entirely to air-side processes. Rather, it appears that energy fluxes from the wave field due to the interaction of the wave field with subsurface currents and turbulence play a significant role once the wave steepness exceeds a critical value. A systematic relationship was observed between low-frequency wave steepness and energy flux from the wave field, normalized in terms of total wind stress and wave speed.

The combination of opposing wind and wind-induced water-side motions is far more effective in attenuating waves than has previously been envisaged. This is qualitatively supported by the field observations of Wright *et al.* (2001). However, there can be significant differences between wind forcing for field and laboratory conditions. For example, under laboratory conditions typically $c/u_*^a \ll 10$ whilst for waves in the open ocean at the spectral peak values of $c/u_*^a > 10$ would be anticipated. Two normalizations of wave attenuation rates are suggested by the data gathered during this study:

$$\frac{\gamma_a}{f} = 2.275(ak)^{0.238}\left|\frac{u_*^a}{c}\right|^{2.112} \quad \text{and} \quad \frac{\partial E}{\partial t} = -115c\rho_{air}\,u_*^{a^2}\,ak^{2.2}.$$

When applied to ocean swells of relatively low steepness, these yield attenuation rates that differ by over an order of magnitude. Determination of appropriate forms for field conditions must await suitable studies utilizing field data sets.

Further studies to expose the underlying causes of these observed attenuation rates are necessary. Measurements of turbulent behaviour within wind-ruffled paddle wave crests moving in opposition to the wind direction are a desirable first step. If, as it appears, wave–turbulence interactions may also be important during the wave growth phase, detailed measurements of the wind input to low-frequency wave growth and attenuation are also required. The techniques developed by Peirson (1997) could profitably be applied to such wave fields to quantify potential tangential stress contributions.

To date, the impact of oblique wind forcing on waves has not been investigated. This study suggests that the response of the wave field to oblique winds could also be strongly dissipative. Detailed investigations of wave field response to oblique winds should also be undertaken.

The authors would like to acknowledge gratefully the support of the United States Army Corps of Engineers through the European Research Office under contract number R&D 9020-EN-1. The initial experiments were undertaken by Mr James Carley. Technical assistance was provided by Messrs John Baird, John Hart and Mark Groskops. Useful discussions with Associate Professor Ron Cox, Professor Michael Banner and Dr Bruce Cathers are also gratefully acknowledged.

REFERENCES

Acton, F. S. 1959 *Analysis of Straight-Line Data*. Wylie.

Banner, M. L. 1990 The influence of wave breaking on the surface pressure distribution in wind-wave interactions. *J. Fluid Mech.* **211**, 463–495.

Banner, M. L. & Peirson, W. L. 1998 Tangential stress beneath wind-driven air-water interfaces. *J. Fluid Mech.* **364**, 115–145.

Belcher, S. E., Harris, J. A. & Street, R. L. 1994 Linear dynamics of wind waves in coupled turbulent air-water flow. *J. Fluid Mech.* **271**, 119–151.

Belcher, S. E. & Hunt, J. C. R. 1998 Turbulent flow over hills and waves. *Annu. Rev. Fluid Mech.* **30**, 507–538.

Bliven, L. F., Huang, N. E. & Long, S. R. 1986 Experimental study of the influence of wind on Benjamin-Feir sideband instability. *J. Fluid Mech.* **162**, 237–260.

Bole, J. B. & Hsu, E. Y. 1969 Response of gravity waves to wind excitation. *J. Fluid Mech.* **35**, 657–675.

Bowers, J. A., Morton, I. D. & Mould, G. I. 2000 Directional statistics of the winds and waves. *App. Ocean Res.* **22**, 13–30.

CERC 1984 *The Short Protecton Manual*. Volume 1. Coastal Engineering Research Center, US Army Corps of Engineers. Vicksburg, MS.

Cheng, Z. & Mitsuyasu, H. 1992 Laboratory studies of the surface drift current induced by wind and swell. *J. Fluid Mech.* **243**, 247–259 (referred to herein as CM92).

Cheung, T. K. & Street, R. L. 1988 The turbulent layer in the water at an air-water interface. *J. Fluid Mech.* **194**, 133–151.

Cohen, J. E. 1997 Theory of turbulent wind over fast and slow waves. PhD Thesis, University of Cambridge.

Dobson, F. W. 1971 Measurement of atmospheric pressure on wind-generated sea waves. *J. Fluid Mech.* **48**, 91–127.

Donelan, M. A. 1990 Air-sea interaction. In *The Sea: Ocean Engineering Science*, Vol. 9 (ed. B. Lemehante & D. M. Hanes), pp. 239–292. Wiley Interscience.

Donelan, M. A. 1999 Wind-induced growth and attenuation of laboratory waves. In *Wind-Over-Wave Couplings, Perspectives and Prospects* (ed. S. G. Sajjadi, N. H. Thomas & J. C. R. Hunt). Clarendon (referred to herein as D99).

Harris, J. A., Fulton, I. & Street, R. L. 1995 Decay of waves in an adverse wind. *Proc. Sixth Asian Congress of Fluid Mechanics, May 22–26, 1995, Singapore.*

Hasselmann, D. & Bösenberg, J. 1991 Field measurements of wave-induced pressure over wind-sea and swell. *J. Fluid Mech.* **230**, 391–428.

Hasselmann, S., Bennefeld, C., Graber, H., Hauser, D., Jackson, F. C., Vachon, P. W., Walsh, E. J., Hasselmann, K. & Long, R. B. 1998 Intercomparison of two-dimensional wave spetra obtained from microwave instruments, buoys and WAModel simulations during the Surface Wave Dynamics Experiment. *Max Planck Institute for Meteorology Rep.* 258. ISSN 0937-1060.

Jiang, J. S., Street, R. L. & Klotz, S. P. 1990 A study of wave-turbulence interaction by use of a nonlinear water wave decomposition technique. *J. Geophys. Res.* **95**, 16037–16054.

Kawai, S. 1981 Visualisation of air-flow separation over wind-wave crests under moderate wind. *Boundary-Layer Met.* **21**, 91–104.

Komen, G. J., Cavaleri, M., Donelan, M., Hasselmann, K., Hasselmann, S. & Janssen, P. A. E. M. 1994 *Dynamics and Modelling of Ocean Waves*. Cambridge University Press.

Longuet-Higgins, M. S. 1969 A non-linear mechanism for the generation of sea waves. *Proc. R. Soc. Lond.* A **311**, 371–389.

Longuet-Higgins, M. S., Cartwright, D. E. & Smith, N. D. 1963 Observations of the direction spectrum of sea waves using the motions of a floating buoy. In *Ocean Wave Spectra*, pp. 111–136. Prentice-Hall.

Mastenbroek, C. 1996 Wind wave interaction. PhD thesis, Delft Technical University.

Mastenbroek, C., Makin, V. K., Garat, M. H. & Giovanangeli, J. P. 1996 Experimental Evidence of the rapid distortion of turbulence in the air flow over water waves. *J. Fluid Mech.* **318**, 273–302.

Mitsuyasu, H. & Honda, T. 1982 Wind-induced growth of water waves. *J. Fluid Mech.* **123**, 425–442 (referred to herein as MH82).

Peirson, W. L. 1997 Measurement of surface velocities and shears at a wavy air-water interface using particle image velocimetry. *Exps. Fluids* **23**, 427–437.

Plant, W. J. 1982 A relationship between wind stress and wave slope. *J. Geophys. Res.* **87**, 1961–1967.

Shemdin, O. H. & Hsu, E. Y. 1967 Direct Measurements of aerodynamic pressure above a simple progressive gravity wave. *J. Fluid Mech.* **30**, 403–416.

Snyder, R. L., Dobson, F. W., Elliott, J. A. & Long, R. B. 1981 Array measurements of atmospheric pressure fluctuations above surface gravity waves. *J. Fluid Mech.* **102**, 1–59.

Van Dorn, W. G. 1966 Boundary dissipation of oscillatory waves. *J. Fluid Mech.* **24**, 769–779.

Teixeira, M. A. C. & Belcher, S. E. 2002 On the distortion of turbulence by a progressive surface wave. *J. Fluid Mech.* **458**, 229–267.

Thais, L. & Magnaudet, J. 1996 Turbulent structure beneath surface gravity waves sheared by wind. *J. Fluid Mech.* **328**, 313–344.

Wright, C. W., Walsh, E. J., Vandemark, D., Krabill, W. B., Garcia, A. W., Houston, S. H., Powell, M. D., Black, P. G. & Marks, F. D. 2001 Hurricane directional wave spectrum spatial variation in the open ocean, *J. Phys. Ocean Ogr.* **31**, 2472–2488.

Young, I. R. & Sobey, R. J. 1985 Measurements of the wind-wave energy flux in an opposing wind. *J. Fluid Mech.* **151**, 427–442.